VECC/NTH 97013

Photons from Hadronic Matter at Finite Temperature

Sourav Sarkar, Jan-e Alam, Pradip Roy
Variable Energy Cyclotron Centre, 1/AF Bidhan Nagar, Calcutta 700 064 India
Abhee K. Dutt-Mazumder, Binayak Dutta-Roy
Saha Institute of Nuclear Physics, 1/AF Bidhan Nagar, Calcutta 700 064 India
Bikash Sinha
Variable Energy Cyclotron Centre, 1/AF Bidhan Nagar, Calcutta 700 064 India
Saha Institute of Nuclear Physics, 1/AF Bidhan Nagar, Calcutta 700 064 India

Abstract

Temperature dependence of hadronic decay widths and masses are studied within the framework of an effective Lagrangian approach. At finite temperature the hadronic masses do not seem to follow a universal scaling law. Considering an exhaustive set of hadronic reactions and vector meson decays we have estimated the photon spectrum emitted from hot hadronic matter taking into account medium effects through thermal loop corrections on the hadronic decay widths and masses. An enhancement in photon emission rate is obtained when we use the in-medium masses of vector mesons in our calculations. It is observed that the effect of ρ decay width on the photon spectra is negligible.

PACS: 25.75.+r;12.40.Yx;21.65.+f;13.85.Qk

Keywords: Heavy Ion Collisions, Vector Mesons, Self Energy, Thermal Loops, Photons.

I. Introduction

Investigation of photons emanating from hot and dense hadronic matter formed in ultra-relativistic heavy-ion collisions is a field of considerable current interest. As the temperature and/or density of hadronic matter increases, it is expected that the system undergoes a phase transition to a new state - quark-gluon plasma (QGP) [1, 2, 3], in which the quarks and gluons are locally free. Electromagnetic probes (photons and dileptons) have been proposed [4] as one of the most promising signals of QGP formation; because of the very nature of their fundamental interactions, they tend to leave the system without much change in their initial energy and momentum,

thus, carrying the information of the reaction zone rather more effectively without being masked by the details of the evolution process, unlike what occurs for hadrons which interact strongly with the rest of the system.

According to lattice QCD calculations, the critical temperature for the phase transition is expected to be around 150 - 200 MeV. In an idealised first order phase transition scenario both hadronic matter and QGP would co-exist at the critical temperature until the cooling due to expansion dominates the heating due to liberation of latent heat. The study of QCD phase transition in the laboratory is also important for understanding the evolution of the early universe a micro-second after the Big Bang [5]. It is therefore essential to understand the hadronic properties at temperatures $\sim 150 - 200$ MeV. To clinch evidence for the formation of QGP in its proper perspective it is essential to evaluate the rate of emission of photons from hadronic matter at finite temperature also, as they contribute to the background in the spectrum of photons from the hot matter formed. For the present purpose we confine our attention to high temperature and zero net baryon density (and, therefore, vanishing chemical potential). Thus our discussions relate to future RHIC and LHC experiments rather than the present SPS data. Inclusion of effects emanating from finite chemical potential is relegated to a future communication.

Irrespective of whether QGP is formed or not, hadronic matter formed in ultra-relativistic heavy-ion collisions is expected to be in a highly excited state. Hadronic interactions in a medium at high temperature are not yet understood fully. There are several aspects where finite temperature medium effects may play an important role. For example, spontaneously broken chiral symmetry (a typical characteristic of hadrons in their ground state) is expected to be restored at high temperature [6], which should manifest itself in the thermal shift of the hadronic masses as well as the change in their decay widths. These modifications of hadron properties e.g. mass, decay widths etc, can be studied through hadronic spectra (threshold for particle production depends on the mass of the particle) as well as from photon and dilepton spectra.

The low energy hadronic states require for their description, non-perturbative methods in QCD which are not available to us. However, the effective Lagrangian approach is quite successful in explaining many of the observed properties of hadronic interactions at the low energy scale [7]. In this paper, by and large we follow the Quantum Hadrodynamics (QHD) model as discussed in Ref. [7].

The properties of a meson get modified due to its interaction with real and virtual excitations in the medium. In QHD, the scalar field is responsible for reduction of the nucleon mass. The vector meson mass falls due to the decrease of the nucleon anti-nucleon masses, which appear through thermal loops in the vector meson self energy. In an effective Lagrangian approach the change in the vector meson mass comes from two different effects. On the one hand, the scattering (space-like process [8]) of the probe with the real (on shell) particles present in the medium via vector meson exchange changes the mass of the vector meson. We observe that such an effect brings in a small change in vector meson masses. On the other hand, the effect of the infinite Dirac sea, which can be probed by time-like processes, reduces the vector meson masses once we take into account the medium modifications of the vacuum. Such an effect is included in our calculation by using the reduced nucleon mass in the vacuum polarization. We observe that the vacuum polarization overwhelms the corresponding medium dependent contribution. In Ref. [9] the temperature dependence of the vector meson masses has been studied by using QCD sum rules. According to these calculations the vector meson mass falls with temperature due to modification of the vacuum at finite temperature. In this approach the decrease in the vector meson masses results from the decrease of the quark condensate with temperature.

The change in the vector meson masses and decay widths modifies the photon production cross section as well as the available phase space in a thermalised system. We evaluate the photon spectra from hot hadronic matter with and without temperature dependent masses and decay widths. It is observed that although the effect of temperature dependent decay width is negligible, the effect of the temperature

dependent masses is important in the photon emission rate.

We organise the paper as follows. In section II we calculate temperature dependent properties of the rho and omega mesons within the framework of an effective Lagrangian approach. In section III we present the calculation of photon rates from hot hadronic matter. Section IVa will be utilised to discuss finite temperature effects on hadronic masses and their decay widths. Section IVb will be devoted to the study of the effects of temperature dependent masses and decay widths on photon production rates and in section V, we present a summary and conclusions.

II. Finite Temperature Effects

To study and understand hadronic matter produced in ultra-relativistic heavy-ion collisions at high temperature, finite temperature field theory is the most consistent approach. The propagation of a particle (say ρ or ω) in a heat bath is modified as its pole is shifted, thereby changing the mass of the particle. In the present calculation thermal effects enter through thermal nucleon and pion loops.

In the following, we briefly discuss the effective (dressed) propagators taking into account the in-medium effects. We begin with the Dyson equation:

$$D^{-1}_{\mu\nu} = (D^{0}_{\mu\nu})^{-1} - \Pi_{\mu\nu}, \tag{1}$$

where

$$D^{0}_{\mu\nu} = \frac{-g_{\mu\nu} + k_\mu k_\nu/m_V^2}{k^2 - m_V^2 + i\epsilon} \tag{2}$$

is the free-space (bare) propagator; $k^\mu = (\omega, \mathbf{k})$ is the four-momentum of the propagating particle and m_V is the mass of the vector meson. $\Pi_{\mu\nu}$ is the self energy of the vector meson given by,

$$\Pi^{\mu\nu} = \Pi^{\mu\nu}_{\rm vac} + \Pi^{\mu\nu}_{\rm med}, \tag{3}$$

where

$$\Pi^{\mu\nu}_{\rm vac} = (g^{\mu\nu} - \frac{k^\mu k^\nu}{k^2})\,\Pi_{\rm vac}(k^2) \tag{4}$$

is the Dirac sea contribution to the self energy [10]. In a thermal bath moving with four-velocity u^μ, $\Pi^{\mu\nu}_{\rm med}$ has transverse and longitudinal components [11],

$$\Pi^{\mu\nu}_{\rm med}(\omega, \mathbf{k}) = A^{\mu\nu}\Pi_{T,\rm med} + B^{\mu\nu}\Pi_{L,\rm med}. \tag{5}$$

$A^{\mu\nu}$ and $B^{\mu\nu}$ are the transverse and longitudinal projection tensors given by

$$A^{\mu\nu} = \frac{1}{k^2-\omega^2}\left[(k^2-\omega^2)(g^{\mu\nu}-u^\mu u^\nu) - k^\mu k^\nu - \omega^2 u^\mu u^\nu + \omega(u^\mu k^\nu + k^\mu u^\nu)\right] \tag{6}$$

and,

$$B^{\mu\nu} = \frac{1}{k^2(k^2-\omega^2)}\left[\omega^2 k^\mu k^\nu + k^4 u^\mu u^\nu - \omega k^2(u^\mu k^\nu + k^\mu u^\nu)\right], \tag{7}$$

which obey the relation

$$A^{\mu\nu} + B^{\mu\nu} = g^{\mu\nu} - \frac{k^\mu k^\nu}{k^2}. \tag{8}$$

Using Eqs. (1-8) the effective propagator becomes

$$D_{\mu\nu} = -\frac{A_{\mu\nu}}{k^2 - m_V^2 + \Pi_T} - \frac{B_{\mu\nu}}{k^2 - m_V^2 + \Pi_L} + \frac{k_\mu k_\nu}{k^2\, m_V^2}, \tag{9}$$

Here,

$$\Pi_{T(L)} = \Pi_{T(L),\rm med} + \Pi_{\rm vac}. \tag{10}$$

Thus we see from Eq. (9) that the diagram defining the self energy $\Pi^{\mu\nu}$ in a thermal bath shifts the pole of the propagator. The real part of the self energy is responsible for mass shifting and the imaginary part gives the decay width of the vector meson in the medium. The effective mass of the vector meson in the medium can be obtained from the pole position of the propagator in the limit $\mathbf{k} \to 0$ *i. e.* in the rest frame of the vector meson. In this limit $\Pi_{T,\rm med} = \Pi_{L,\rm med} = \Pi_{\rm med}$, and we have,

$$\frac{1}{3}\Pi^\mu_\mu = \Pi = \Pi_{\rm med} + \Pi_{\rm vac} \tag{11}$$

The effective mass of the vector meson is then obtained by solving the equation:

$$\omega^2 - m_V^2 + {\rm Re}\Pi = 0 \tag{12}$$

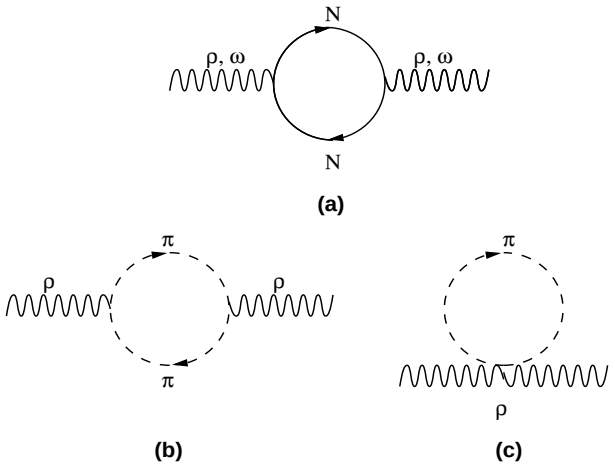

Figure 1: Feynman Diagrams for self energy of vector mesons

IIa. VNN Interaction

To calculate the effective mass and decay widths we begin with the following VNN (Vector - Nucleon - Nucleon) Lagrangian density:

$$\mathcal{L}_{VNN} = g_{VNN}\left(\bar{N}\gamma_\mu\tau^a N V_a^\mu - \frac{\kappa_V}{2M}\bar{N}\sigma_{\mu\nu}\tau^a N\partial^\nu V_a^\mu\right), \tag{13}$$

where $V_a^\mu = \{\omega^\mu, \vec{\rho}^\mu\}$, M is the free nucleon mass, N is the nucleon field and $\tau_a = \{1, \vec{\tau}\}$. The values of the coupling constants g_{VNN} and κ_V will be specified later. With the above Lagrangian we proceed to calculate the ρ-self energy. The relevant Feynman diagram is shown in Fig. (1a). The one-loop correlation function is given by,

$$\Pi_{\mu\nu} = -2ig_{VNN}^2\int\frac{d^4p}{(2\pi)^4}\,S_{\mu\nu}(p,k), \tag{14}$$

with,

$$S_{\mu\nu} = \frac{\mathrm{Tr}\left[\Gamma_\mu(k)\,(\not{p}+M^*)\Gamma_\nu(-k)\,(\not{p}-\not{k}+M^*)\right]}{(p^2-M^{*2})((p-k)^2-M^{*2})}, \tag{15}$$

The vertex $\Gamma_\mu(k)$ is calculated by using the Lagrangian of Eq. (13) and is given by

$$\Gamma_\mu(k) = \gamma_\mu + \frac{i\kappa_V}{2M}\sigma_{\mu\alpha}k^\alpha. \tag{16}$$

Here M^* is the in-medium (effective) mass of the nucleon at finite temperature which we calculate using the Mean-Field Theory (MFT) [7]. The value of M^* can be found by solving the following self consistent equation:

$$M^* = M - \frac{4g_s^2}{m_s^2} \int \frac{d^3\mathbf{p}}{(2\pi)^3} \frac{M^*}{(\mathbf{p}^2 + M^{*2})^{1/2}} \left[f_N(T) + f_{\bar{N}}(T) \right], \tag{17}$$

where $f_N(T)(f_{\bar{N}}(T))$ is the Fermi-Dirac distribution for the nucleon (antinucleon), m_s is mass of the neutral scalar meson (σ) field, and, the nucleon interacts via the exchange of isoscalar meson with coupling constant g_s. Since the exact solution of the field equations in QHD is untenable, these are solved in the mean field approximation. In a mean field approximation one replaces the field operators by their ground state expectation values which are classical quantities [7]; this renders the field equations exactly solvable.

The vacuum part of the ρ self energy arises due to its interaction with the nucleons in the modified Dirac sea. This is calculated using dimensional regularization scheme to yield,

$$\mathrm{Re}\Pi_{\mathrm{vac}}(\omega, \mathbf{k} \to 0) = -\frac{g_{VNN}^2}{\pi^2}\omega^2 \left[I_1 + M^* \frac{\kappa_V}{2M} I_2 + \frac{1}{2} \left(\frac{\kappa_V}{2M}\right)^2 (\omega^2 I_1 + M^{*2} I_2) \right] \tag{18}$$

where,

$$I_1 = \int_0^1 dz\, z(1-z)\, \ln \left[\frac{M^{*2} - \omega^2\, z(1-z)}{M^2 - m_V^2\, z(1-z)} \right], \tag{19}$$

$$I_2 = \int_0^1 dz\, \ln \left[\frac{M^{*2} - \omega^2\, z(1-z)}{M^2 - m_V^2\, z(1-z)} \right]. \tag{20}$$

Here, it is important to note that we have used the in-medium nucleon mass in the vacuum part of the self energy of the vector meson.

In a hot system of particles, there is a thermal distribution of real particles (on shell) which can participate in the absorption and emission process in addition to the exchange of virtual particles. The interaction of the rho with the onshell nucleons, present in the thermal bath contributes to the medium dependent part of the ρ-self energy. This is calculated from Eq.(14) using imaginary time formalism [12, 13] as,

$$\mathrm{Re}\Pi_{\rm med}(\omega, \mathbf{k} \to 0) = -\frac{8 g_{VNN}^2}{\pi^2} \int \frac{p^2\, dp}{\omega_p\, (e^{\beta\,\omega_p}+1)(4\omega_p^2 - \omega^2)} \times \left[\frac{2}{3}(2p^2 + 3M^{*2}) - \omega^2 \left\{2M^*(\frac{\kappa_V}{2M}) - \frac{2}{3}(\frac{\kappa_V}{2M})^2(p^2 + 3M^{*2})\right\}\right] \quad (21)$$

where, $\omega_p^2 = p^2 + M^{*2}$. Note that in the above equation the sign of the term proportional to κ_V is opposite to that obtained in Ref. [14] (see Eq. (14) of Ref. [14]).

IIb. $\rho\pi\pi$ Interaction

The change in the properties of ρ meson due to rho pion coupling has been studied in a similar manner. The effect in this case is small [15] compared to the nucleon loop contribution. This is attributed to the fact that the pion mass does not change in the medium but the nucleon mass drops substantially due to mean-field effects. To evaluate the rho self-energy due to $\pi\pi$ loop we use the following well known interaction Lagrangian:

$$\mathcal{L}_{\rho\pi\pi} = -g_{\rho\pi\pi}\, \vec{\rho}^{\mu} \cdot (\vec{\pi} \times \partial_\mu \vec{\pi}) + \frac{1}{2} g_{\rho\pi\pi}^2 (\vec{\rho}^{\mu} \times \vec{\pi}) \cdot (\vec{\rho}_\mu \times \vec{\pi}) \quad (22)$$

where the vector signs on the ρ and π indicate that they are isovectors.

In this case the diagrams 1(b)and 1(c) contribute to the rho self energy in the hot medium and is given by,

$$\Pi^{\mu\nu} = i g_{\rho\pi\pi}^2 \int \frac{d^4p}{(2\pi)^4} \frac{(2p+k)^\mu (2p+k)^\nu}{[(p+k)^2 - m_\pi^2][p^2 - m_\pi^2]} - 2i g_{\rho\pi\pi}^2 \int \frac{d^4p}{(2\pi)^4} \frac{1}{[p^2 - m_\pi^2]} \quad (23)$$

This is again evaluated using the imaginary time formalism to give,

$$\mathrm{Re}\Pi(\omega, \mathbf{k} \to 0) = -\frac{g_{\rho\pi\pi}^2}{3\pi^2} \int \frac{p^2\, dp}{\omega_p} \left[3 - \frac{4p^2}{4\omega_p^2 - \omega^2}\right] \frac{1}{e^{\beta\omega_p} - 1} \quad (24)$$

Here, $\omega_p^2 = p^2 + m_\pi^2$. We then calculate the change in ρ-mass due to pion loop using Eqs. (12) and (24).

The decay width for the process $\rho \to \pi\,\pi$ can be calculated from the imaginary part of the self energy using cutting rules [16] which, in the rest frame of ρ-meson

is given by (see Appendix - I)

$$\Gamma_{\rho\to\pi\,\pi} = \frac{g_\rho^2}{48\pi\,\omega^2}\,(\omega^2 - 4m_\pi^2)^{3/2}\left[\left(1+n(\frac{\omega}{2})\right)\,\left(1+n(\frac{\omega}{2})\right) - n(\frac{\omega}{2})n(\frac{\omega}{2})\right] \qquad (25)$$

where $\omega = m_\rho^*$ is the in-medium mass of ρ-meson. $n(\omega/2)$ is Bose-Einstien distribution for the π-meson. The first term in Eq.(25) represents the stimulated emission of pions with statistical weight $(1+n(\omega/2))(1+n(\omega/2))$ and the second term stands for the absorption of pions with weight factor $n(\omega/2)n(\omega/2)$.

It has been emphasized recently [17] that the medium effects on the decay width of the ρ-meson play a very important role. The thermal nucleon loop brings about a modification of the ρ-dominated pion form factor which is further influenced by the thermal distributions of the pions at a finite temperature. The medium effects on dilepton spectra through the decay width of ρ-meson has been shown to be very important in Ref. [17]. In our calculation of photon spectra we include such effects through the rho-propagator.

III. Photons from Hot Hadronic Matter

Whether a QCD phase transition takes place or not, photons can be used as a probe to study the properties of hadrons in hot/dense medium. In a phase transition scenario, apart from the QGP, photons are also produced from the thermalised hadronic gas, formed after the phase transition. Substantial contributions to the total photon yield also come from the initial hard collision of partons in the high momentum regime, and from hadronic decays ($\pi^0 \to \gamma\,\gamma, \eta \to \gamma\,\gamma$ etc.) in the low momentum zone. The hard QCD photons can be well understood through perturbative QCD and the decay photons can be reconstructed by invariant mass analysis. Thus, to extract photon signals from QGP it is essential to estimate the photon rates from various hadronic reactions and vector meson decays which is a challenging task, indeed. The temperature of the hadronic phase lies between 150 - 200 MeV. Therefore the finite temperature corrections to the hadronic properties and their consequences on photon spectra are very important.

Many of the aspects of the interacting pion gas have been reported in the literature [18, 19, 20]. For our purpose we model the hadronic gas as consisting of π, ρ, ω and η. First we consider the reactions $\pi\,\pi \rightarrow \rho\,\gamma$, $\pi\,\rho \rightarrow \pi\,\gamma$ and the decay $\rho \rightarrow \pi\pi\gamma$. We estimate the differential cross-section for photon production from the above processes taking into account the finite width of the rho meson (see Appendix - II). The relevant vertices are obtained from the following Lagrangian:

$$\mathcal{L} = -g_{\rho\pi\pi}\vec{\rho}^{\mu} \cdot (\vec{\pi} \times \partial_{\mu}\vec{\pi}) - eJ^{\mu}A_{\mu} + \frac{e}{2}F^{\mu\nu}\,(\vec{\rho}_{\mu} \times \vec{\rho}_{\nu})_3, \tag{26}$$

where $F_{\mu\nu} = \partial_{\mu}A_{\nu} - \partial_{\nu}A_{\mu}$, is the Maxwell field tensor and J^{μ} is the hadronic part of the electromagnetic current given by

$$J^{\mu} = (\vec{\rho}_{\nu} \times \vec{B}^{\nu\mu})_3 + (\vec{\pi} \times (\partial^{\mu}\pi + g_{\rho\pi\pi}\vec{\pi} \times \vec{\rho}^{\mu}))_3 \tag{27}$$

with $\vec{B}_{\mu\nu} = \partial_{\mu}\vec{\rho}_{\nu} - \partial_{\nu}\vec{\rho}_{\mu} - g_{\rho\pi\pi}(\vec{\rho}_{\mu} \times \vec{\rho}_{\nu})$, and the subscript 3 after the cross product indicates the relevant component in isospin space. The last term in Eq. (26) as well as the first term in Eq. (27) arise due to the non-abelian structure of the $SU(2) \times U(1)$ gauge group [7]. The 2ρ-1γ vertex has been calculated by using the last two terms of the lagrangian (26) to obtain gauge invariant amplitudes.

We have also considered the photon production due to the reactions $\pi\,\eta \rightarrow \pi\,\gamma$, $\pi\,\pi \rightarrow \eta\,\gamma$ and the decay $\omega \rightarrow \pi\,\gamma$ using the following Lagrangian [21, 22]:

$$\mathcal{L} = \frac{g_{\rho\rho\eta}}{m_{\eta}}\,\epsilon_{\mu\nu\alpha\beta}\partial^{\mu}\rho^{\nu}\partial^{\alpha}\rho^{\beta}\eta + \frac{g_{\omega\rho\pi}}{m_{\pi}}\,\epsilon_{\mu\nu\alpha\beta}\partial^{\mu}\omega^{\nu}\partial^{\alpha}\rho^{\beta}\pi^{0} + \frac{em_{\rho}^{2}}{g_{\rho\pi\pi}}A_{\mu}\rho^{\mu} \tag{28}$$

The last term in the above Lagrangian is written down on the basis of Vector Meson Dominance (VMD) [23].

In the case of nuclear collisions, one is more interested in overall photon rates rather than the cross-sections. The rate of emission of thermal photons with energy E and momentum p is given by

$$E\frac{dR}{d^3p} = -\frac{2g^{\mu\nu}}{(2\pi)^3}\mathrm{Im}\Pi^{R}_{\mu\nu}\,(p)\frac{1}{e^{\beta E} - 1} \tag{29}$$

where $\mathrm{Im}\Pi^{R}_{\mu\nu}$ is the imaginary part of the retarded photon self energy at finite temperature. The emission rate given by Eq. (29) is correct upto order e^2 in electromagnetic interaction but exact (albeit in principle) to all orders in strong interaction. If

$\mathrm{Im}\Pi^R_{\mu\nu}$ is evaluated by carrying out loop expansion up to a finite order and applying the cutting rules (*á lá* finite temperature modification of the Cutkosky-Landau prescriptions) [16] then the photon emission rate becomes equivalent to the one obtained in relativistic kinetic theory formalism [15]. It may be worthwhile to mention that for a typical photon producing reaction (x particles $\rightarrow$ y particles $+\gamma$), the above two formalisms will give equivalent results if the photon self-energy is approximated by carrying out a loop expansion upto and including L loops where L satifies $x + y < L + 1$ [15].

In this article we compute the rate of photon production per unit volume at a temperature T using the relativistic kinetic theory approach [24],

$$E\frac{dR}{d^3p} = \frac{\mathcal{N}}{16(2\pi)^7 E}\int_{(m_1+m_2)^2}^{\infty} ds \int_{t_{\min}}^{t_{\max}} dt\,|\mathcal{M}|^2 \int dE_1 \times \int dE_2 \frac{f(E_2)\,f(E_2)\,[1+f(E_3)]}{\sqrt{aE_2^2+2bE_2+c}} \tag{30}$$

where $\mathcal{M}$ is the invariant amplitude (see Appendix II) of photon production for the appropriate reaction channel, evaluated from the Lagrangians given by Eqs. (26) and (28). It may be emphasized that here, as elsewhere in the literature, unstable external particles are taken to be on-shell with medium modified masses. For convenience we show the parameters a, b, c and also the limits of the integrals in Appendix III.

IV. Results

IVa. Finite Temperature Properties

In this section we present the results of our calculation of the effective masses and decay widths of vector mesons. For our calculations of ρ-meson effective mass we have used the following values of the coupling constants and masses [25]: $\kappa_\rho = 6.1$, $g^2_{\rho NN}/4\pi = 0.55, m_s$= 550 MeV, $m_\rho = 770$ MeV, $M = 938$ MeV, and $g_s^2/4\pi = 9.3$. The variation of nucleon mass due to the mean field plays a vital role in determining the effective mass of ρ and ω mesons. The effective mass of the nucleon is calculated from Eq. (17) and its variation with temperature is plotted in Fig. (2).

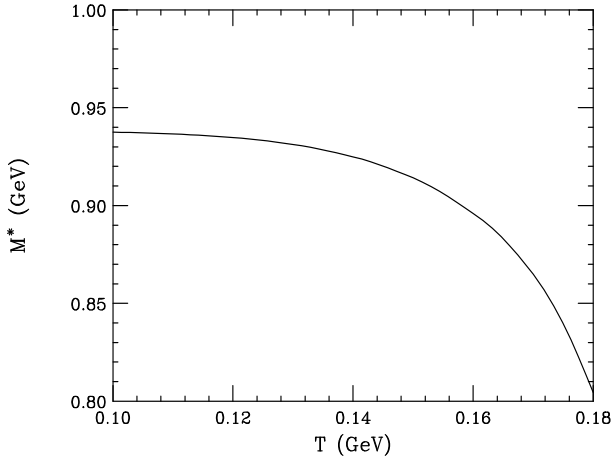

Figure 2: Effective nucleon mass (M^*) as a function of temperature (T).

It is seen that the nucleon mass remains almost constant upto a temperature of 140 MeV beyond which it starts falling. We have plotted our results upto a temperature of 180 MeV above which the effective nucleon mass decreases very sharply.

We now consider the effect of $N\bar{N}$ polarisation on the ρ-meson mass. The vacuum and in-medium contributions are shown separately in Fig. (3). We observe that the in-medium contribution increases very little ($\sim 5 - 10$ MeV) with temperature from its free space value. This is similar to the result reported by Song *et. al* [14]. The overall decrease ($\approx 32\%$ at $T = 180$ MeV) in the effective mass can be attributed almost entirely to fluctuations in the Dirac sea of nucleons with mass M^*. The effective mass of the ρ due to $\pi\pi$ polarisation is also shown in the inset of Fig. (3). In this case we observe a very small (2%) increase in the effective mass at T =180 MeV.

To calculate the effective mass of ω-meson, we take $g^2_{\omega NN}/4\pi = 20$, $\kappa_\omega = 0$ [25]. The result is shown in Fig. (4). We observe the same feature as Fig. (3) with an increase of about 70 MeV at $T = 180$ MeV in the in-medium contribution. The overall decrease in omega mass at T =180 MeV is about 200 MeV from its free space value.

Many authors have investigated the issue of temperature dependence of hadronic masses within different models over the past several years. Hatsuda and collabo-

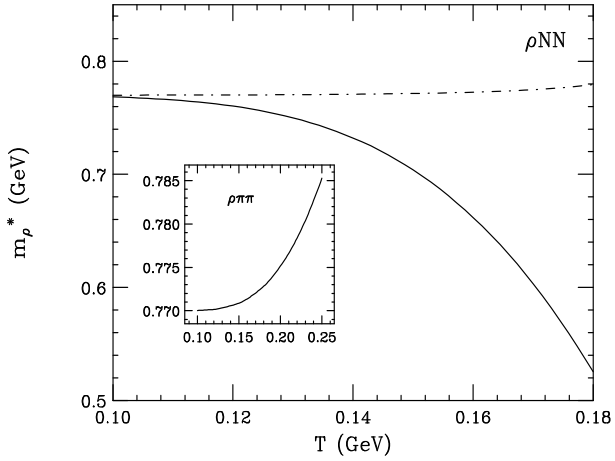

Figure 3: Effective rho mass (m^*_ρ) as a function of temperature (T). The dot-dashed line shows the effective mass due to $N\bar{N}$ polarisation at finite temperature whereas the solid line includes the effect of fluctuations of the Dirac sea of nucleons with mass M^*. The inset shows the effective rho mass due to $\pi\pi$ polarisation at finite temperature.

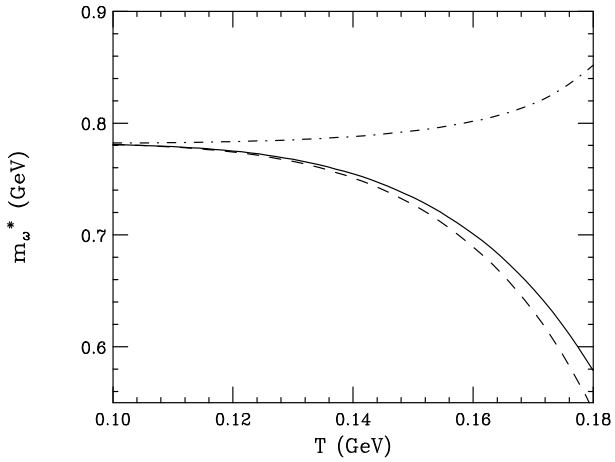

Figure 4: Effective omega mass (m^*_ω) as a function of temperature (T). The dot-dashed line shows the effective mass due to $N\bar{N}$ polarisation at finite temperature and the dashed line shows the effect of fluctuations of the Dirac sea of nucleons with mass M^*. Solid line represents the net effect.

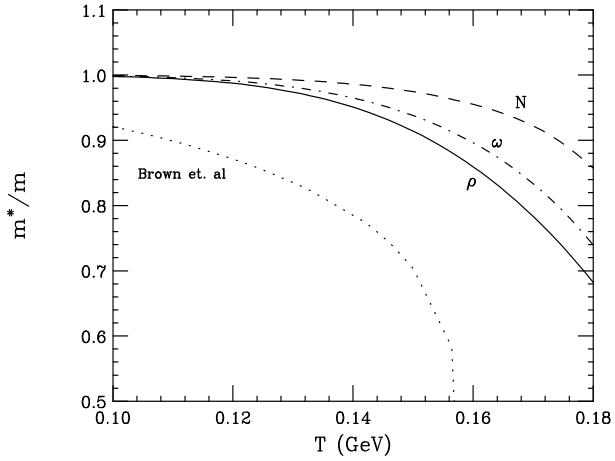

Figure 5: Ratio of effective mass to free space mass of hadrons as a function of temperature T.

rators [26, 27, 28] and Brown [29] showed that the use of QCD sum rules at finite temperature results in a temperature dependence of the $q\bar{q}$ condensate culminating in the following behaviour of the ρ-mass:

$$\frac{m_\rho^*}{m_\rho} = \left(1 - \frac{T^2}{T_\chi^2}\right)^{1/6} \tag{31}$$

where T_χ is the critical temperature for chiral phase transition. Brown and Rho [30] also showed that the requirement of chiral symmetry yields an approximate scaling relation between various effective hadron masses,

$$\frac{M^*}{M} \approx \frac{m_\rho^*}{m_\rho} \approx \frac{m_\omega^*}{m_\omega} \approx \frac{f_\pi^*}{f_\pi} \tag{32}$$

These calculations show a dropping of hadronic mass with temperature. Calculations with non-linear σ-model, however, predict the opposite trend [31]. In order to make a comparative study we plot the ratios of the effective masses to the free masses of ρ, ω and N versus temperature in Fig. (5). The expected trend based on Brown - Rho scaling is also shown. Firstly, we do not observe any global scaling behaviour. Secondly, in our case the effective mass as a function of temperature falls at a slower rate.

The variation of the in-medium decay width (Γ_ρ) of the rho meson with temperature is shown in Fig. (6). As discussed earlier, the effective mass of the rho

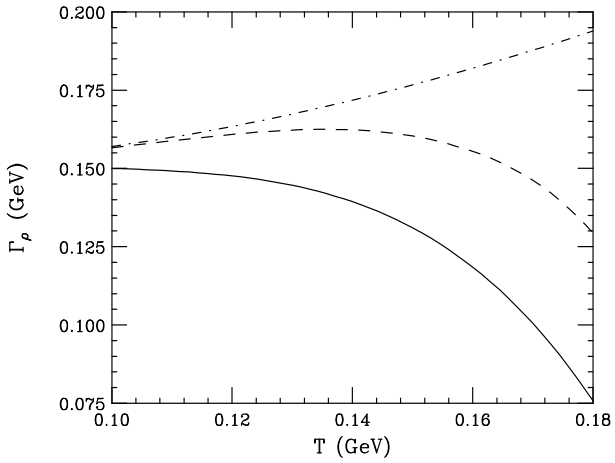

Figure 6: Rho decay width (Γ_ρ) as a function of temperature (T). Dashed and solid lines show calculations of rho width with effective mass due to nucleon loop, with and without BE. Dot dashed line represents the same but with effective mass due to pion loop.

decreases as a result of $N\bar{N}$ polarisation. This reduces the phase space available for the rho. Hence, we observe a rapid decrease in the rho meson width with temperature (solid line). However, the presence of pions in the medium would cause an enhancement of the decay width through induced emission. Thus when Bose Enhancement (BE) of the pions is taken into account the rho decay width is seen to fall less rapidly (dashed line); such a behaviour is observed quite clearly in [17]. For the sake of completeness, we also show the variation of rho width in the case where the rho mass changes due to $\pi\pi$ loop. In this case, since the rho mass increases (though only marginally), the width increases (dot-dashed line).

IVb. Photon Spectra

In this section we present our results on photon emission rates from a hot hadronic gas. As discussed earlier, the variation of hadronic decay widths and masses will affect the photon spectra. The relevant reactions of photon production are $\pi\pi \rightarrow \rho\,\gamma, \pi\,\rho \rightarrow \pi\,\gamma, \pi\,\pi \rightarrow \eta\,\gamma$, and $\pi\,\eta \rightarrow \eta\,\gamma$ with all possible isospin combinations. Since the lifetimes of the rho and omega mesons are comparable to the strong interaction time scales, the decays $\rho \rightarrow \pi\,\pi\,\gamma$ and $\omega \rightarrow \pi^0\,\gamma$ are also included.

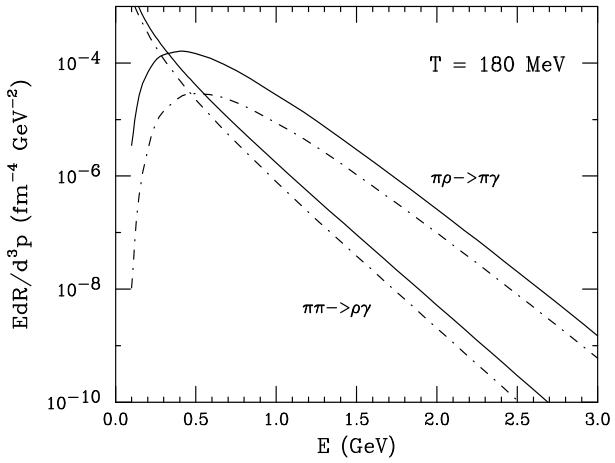

Figure 7: Photon emission rates from $\pi\pi \rightarrow \rho\gamma$ and $\pi\rho \rightarrow \pi\gamma$ as a function of photon energy at T=180 MeV. The solid and dot-dashed lines show results with and without in-medium effects respectively.

Contributions from $\rho \rightarrow \pi\,\gamma$ and $\omega \rightarrow \pi\,\pi\,\gamma$ are ignored because of very small decay widths of these processes. We will consider the first two reactions in detail since they are seen to dominate the total photon yield. The effect of finite resonance width of the rho meson in the photon production cross-sections has been taken into account through the propagator, which was neglected in Ref. [22].

In Fig. (7) the photon emission rates from the first two reactions ($\pi\,\pi \rightarrow \rho\,\gamma$ and $\pi\,\rho \rightarrow \pi\,\gamma$) with and without finite temperature effects are presented at T = 180 MeV. When in-medium masses and decay widths are taken into account, the photon yields from both the reactions are found to increase compared to the case when free masses and widths are considered. To understand this, let us recall that the emission rate of photons from a reaction $h_1\,h_2 \rightarrow h_3\,\gamma$ can be approximated as [3]

$$E\frac{dR}{d^3p} \propto f_{h_1}(p_\gamma) \int ds\, \frac{dE_{h_2}}{E_\gamma}\, f_{h_2}(1+f_{h_3}) \times \sqrt{s(s-4m^2)}\,\sigma_{h_1 h_2 \rightarrow h_3\,\gamma} \tag{33}$$

where m is the mass of the particles in the incident channel ($= m_{h_1} = m_{h_2}$). Observe that the in-medium effects on the photon yield may come from both the cross-section and the phase-space factor. Consider the reaction $\pi\,\pi \rightarrow \rho\,\gamma$. From simple

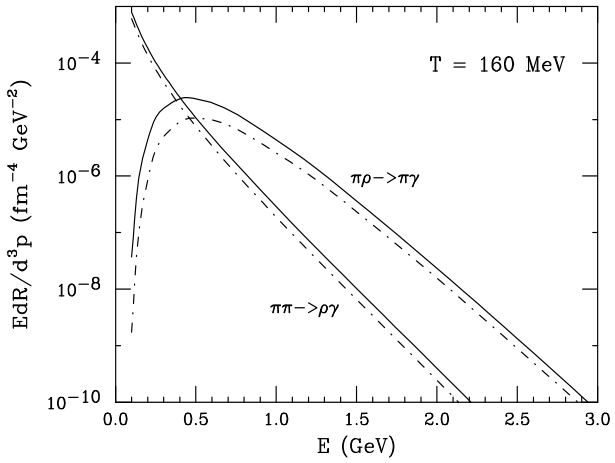

Figure 8: Photon emission rates from $\pi\pi \rightarrow \rho\gamma$ and $\pi\rho \rightarrow \pi\gamma$ as a function of photon energy at T=160 MeV. The solid and dot-dashed lines show results with and without in-medium effects respectively.

kinematics we calculate the energy carried by the photon as $E_\gamma = (\sqrt{s} - m_\rho^2/\sqrt{s})/2$. When the rho mass drops, the possibility of getting a photon of higher energy increases for a given centre of mass energy of the $\pi\pi$ system. The increase in photon emission rate with medium effects, hence, is due to the increase in the basic cross section $\sigma_{\pi\pi\rightarrow\rho\gamma}$. The effect of the phase space factor is rather small in this case.

In the case of the reaction $\pi\,\rho \rightarrow \pi\gamma$, the phase-space factor plays a very crucial role. At low energy ($E \leq 0.5$ GeV) the photon yield with medium effects is found to increase by an order of magnitude. At higher energies the enhancement is by a factor $\sim$ 2 - 3. At lower temperature, the medium effects on the photon spectra should be smaller which is borne out very clearly from our calculations, as shown in Fig. (8). At higher photon energies (> 0.5 GeV) the reaction $\pi\rho \rightarrow \pi\gamma$ dominates over $\pi\pi \rightarrow \rho\gamma$ because for a fixed energy ($\sqrt{s}$) in the centre of mass system of the colliding particles the production of heavier meson (ρ) leaves lesser phase-space than that for the reaction where the lighter one (π) is in the final channel. In other words, in $\pi\rho \rightarrow \pi\gamma$ the heavier meson in the incident channel appears as a massless boson (γ) in the final channel making available a large amount of rest mass energy of the ρ to the kinetic energy of the photon.

The photon emission rate from the decay $\rho \rightarrow \pi\,\pi\,\gamma$ in the high energy region

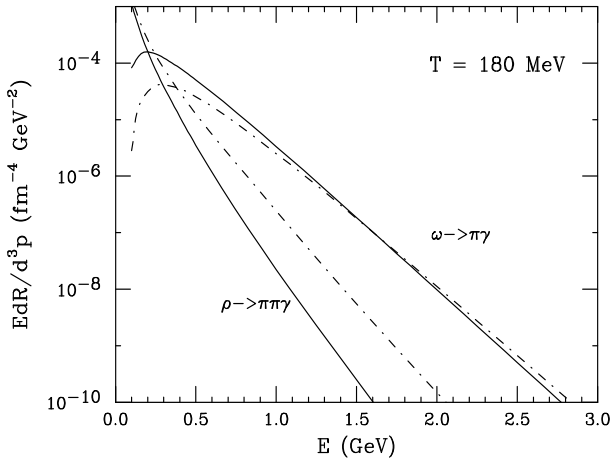

Figure 9: Photon emission rates from $\rho \to \pi\pi\gamma$ and $\omega \to \pi\gamma$ as a function of photon energy at T=180 MeV. The solid and dot-dashed lines show results with and without in-medium effects respectively.

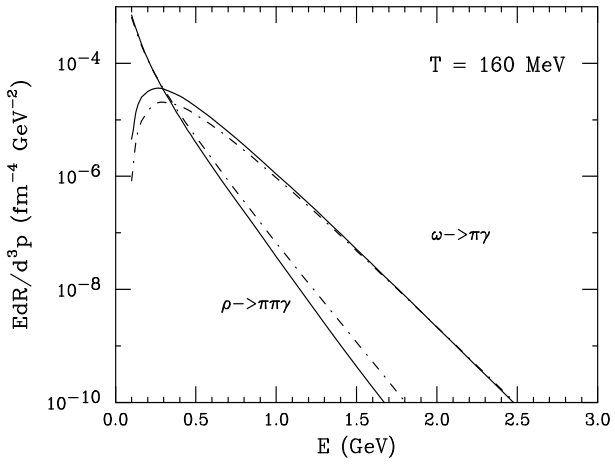

Figure 10: Photon emission rates from $\rho \to \pi\pi\gamma$ and $\omega \to \pi\gamma$ as a function of photon energy at T=160 MeV. The solid and dot-dashed lines show results with and without in-medium effects respectively.

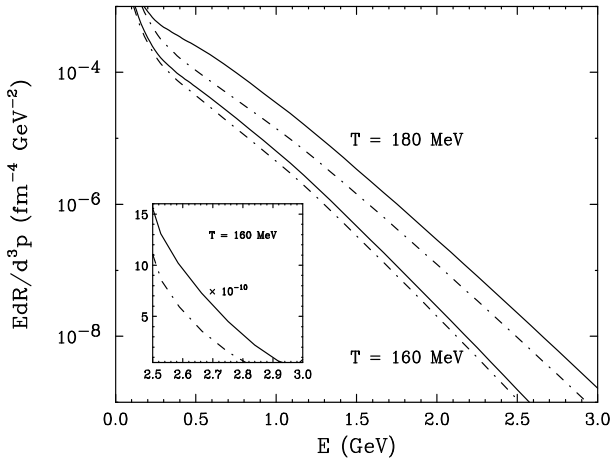

Figure 11: Total photon emission rate from hot hadronic matter as a function of photon energy at T=160, 180 MeV. The solid and dot-dashed lines show results with and without in-medium effects respectively. Inset: Total photon emission rate is plotted in linear scale as a function of photon energy in the kinematic window, $E_\gamma = 2.5$ to 3.0 GeV at T =180 MeV.

reduces due to the decrease of the rho mass in the incident channel as seen in Figs. (9) and (10). The corresponding results for ω decay are also shown. In the case of ω decay the total energy in the final channel is shared by two particles whereas in the case of ρ decay there are three particles in the final channel, therefore the former dominates over the later at high photon energies.

In Fig. (11) we display the total rate of emission of photons from hot hadronic gas including all hadronic reactions and decays of vector mesons. At T =180 MeV, the photon emission rate with finite temperature effects is a factor of ~ 3 higher than the rate calculated without medium effects. At $T = 160$ MeV the medium effects are small compared to the previous case.

V. Summary and Conclusions

In this work we have calculated the effective masses and decay widths of vector mesons propagating in a hot medium. We have seen that the mass of rho meson decreases substantially due to its interactions with nucleonic excitations and it increases only marginally ($\sim$ 10-15 MeV) due to $\rho - \pi$ interactions. The overall

decrease in the effective mass is due to fluctuations in the modified Dirac sea of nucleons with mass M^*. For ω mesons the in-medium contribution increases by 70 MeV at T =180 MeV but the Dirac sea effect overwhelms the medium effect and consequently the effective omega mass drops at T =180 MeV by about 200 MeV from its free space value.

We have evaluated the rate of photon emission from a hadronic gas of π, ρ, ω and η mesons. It is seen that photon rate increases by a factor ~ 3 due to the inclusion of in-medium masses at T =180 MeV. We observe that the inclusion of in-medium decay width in the vector meson propagator has negligible effect on the photon emission rates, although the effect of the in-medium decay width with BE is substantial for the dilepton yield [17]. It may be remarked that the present paper deals with a zero net baryon density situation and is thus appropriate for future experiments at RHIC and LHC. Inclusion of effects arising from finite chemical potential shall be communicated in a separate paper.

The observed photon spectra should be obtained by folding the static rate with the expansion dynamics. An ideal hydrodynamical model (e.g. Bjorken hydrodynamics [32]) for the space time evolution does not appear to be adequate here because of the following reason. When the temperature of the medium is large, the hadron masses are reduced and the amount of mass decreased will appear as energy of the field; as the system expands and consequently cools the hadrons regain their masses gradually from the field energy. This could have non-trivial effects on the equation of state of the system and one needs a more realistic hydrodynamic model to handle the evolution dynamics. Hydrodynamic flow with changing hadronic properties is a subject of much contemporary interest and we are pursuing it presently [33].

Acknowledgement:

We are grateful to P. Lichard and R. Rapp for useful discussions, and also to the referee whose comments were extremely helpful.

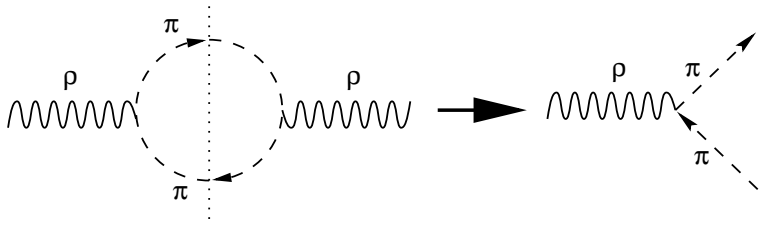

Figure 12: Decay of rho meson.

Appendix - I: Rho Decay Width

We have calculated the decay width of the rho meson using the Cutkosky rules at finite temperature (see Fig. (12)) which give a simple and systematic way to calculate the imaginary part of the rho self-energy. This is related to the physical decay width of the rho as

$$\mathrm{Im}\Pi(\omega) = -\omega\Gamma(\omega) \tag{34}$$

The rho self-energy develops cuts along the real axis when the pions become on-mass shell and the discontinuity across these cuts is pure imaginary for real ω so that we have

$$\mathrm{Disc}\Pi(\omega) = [\Pi(\omega + i\epsilon) - \Pi(\omega - i\epsilon)] = 2i\mathrm{Im}\Pi(\omega) \tag{35}$$

From Eq. (23) and the identity,

$$\begin{aligned} \frac{1}{\beta}\sum_{n=-\infty}^{+\infty} f(p_0 = 2\pi i n T) &= \frac{1}{2\pi i}\int_{-i\infty}^{i\infty}\frac{1}{2}[f(p_0) + f(-p_0)]dp_0 \\ &+ \frac{1}{2\pi i}\int_{-i\infty+\epsilon}^{i\infty+\epsilon}[f(p_0) + f(-p_0)]\frac{dp_0}{e^{\beta p_0} - 1}, \end{aligned} \tag{36}$$

we have,

$$\begin{aligned} \Pi(\omega) &= \frac{1}{3}\Pi^{\mu}_{\mu}(\omega, \mathbf{k} \to 0) \\ &= \frac{g^2_{\rho\pi\pi}}{6\pi^2}\int\frac{p^2 dp}{\omega_p}\left[1 + \frac{4p^2}{4\omega_p^2 - \omega^2}\right][2n(\omega_p) + 1] \end{aligned} \tag{37}$$

In the above equation $\omega = m^{\star}_{\rho}$ is the effective mass of the ρ - meson. Hence,

$$\begin{aligned} \mathrm{Disc}\Pi(\omega) &= \frac{ig^2_{\rho\pi\pi}}{3\pi}\int\frac{p^4 dp}{\omega_p^2}[2n(\omega_p) + 1] \\ &\times[\delta(\omega + 2\omega_p) - \delta(\omega - 2\omega_p)] \end{aligned} \tag{38}$$

From Eqs. (35) and (38) we have

$$\mathrm{Im}\Pi(\omega) = -\frac{g^2_{\rho\pi\pi}}{48\pi\omega}(\omega^2 - 4m_\pi^2)^{3/2}\left[\left\{2n(\frac{\omega}{2})+1\right\} - \left\{2n(-\frac{\omega}{2})+1\right\}\right] \qquad (39)$$

We are interested in the decay width $\Gamma_{\rho\to\pi\,\pi}$ and the diagram which contributes to this is shown in Fig. (12). The corresponding decay width can be read out from the above equation:

$$\Gamma_{\rho\to\pi\,\pi}(T) = \frac{g^2_{\rho\pi\pi}}{48\pi\omega^2}(\omega^2 - 4m_\pi^2)^{3/2}\left[2n(\frac{\omega}{2})+1\right] \qquad (40)$$

Appendix - II: Invariant Amplitudes

In this appendix we present the invariant amplitudes for photon productions from the Lagrangian given by Eq. (26).

$$\underline{(1)\ \pi^+(p_1) + \pi^-(p_2)\ \to\ \rho^0(p_3) + \gamma(p_4)}$$

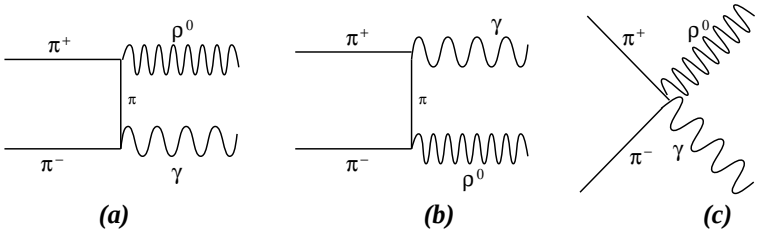

Figure 13: Feynman diagrams for $\pi^+\pi^- \to \rho^0\gamma$

$$\begin{aligned}
\mathcal{M}_{\dashv} &= -\frac{4eg_{\rho\pi\pi}}{(t-m_\pi^2)}p_{1\mu}p_{2\nu}\epsilon^{*\mu}(p_3)\epsilon^{*\nu}(p_4) \\
\mathcal{M}_{\lfloor} &= -\frac{4eg_{\rho\pi\pi}}{(u-m_\pi^2)}p_{1\mu}p_{2\nu}\epsilon^{*\nu}(p_3)\epsilon^{*\mu}(p_4) \\
\mathcal{M}_{\rfloor} &= -2eg_{\rho\pi\pi}g_{\mu\nu}\epsilon^{*\mu}(p_3)\epsilon^{*\nu}(p_4)
\end{aligned}$$

$$\begin{aligned}
\overline{|\mathcal{M}_a|^2} &= \frac{16e^2g^2_{\rho\pi\pi}}{(t-m_\pi^2)^2}\,m_\pi^2\left[m_\pi^2 - \frac{(m_\pi^2+m_\rho^2-t)^2}{4m_\rho^2}\right] \\
\overline{|\mathcal{M}_b|^2} &= \frac{16e^2g^2_{\rho\pi\pi}}{(u-m_\pi^2)^2}\,m_\pi^2\left[m_\pi^2 - \frac{(m_\pi^2+m_\rho^2-u)^2}{4m_\rho^2}\right] \\
\overline{|\mathcal{M}_c|^2} &= 12e^2g^2_{\rho\pi\pi}
\end{aligned}$$

$$
\begin{aligned}
2\mathrm{Re}\overline{[\mathcal{M}_a^*\mathcal{M}_b]} &= \frac{8e^2g_{\rho\pi\pi}^2(s-2m_\pi^2)}{(t-m_\pi^2)(u-m_\pi^2)}\left[(s-2m_\pi^2)-\frac{(m_\pi^2+m_\rho^2-t)(m_\pi^2+m_\rho^2-u)}{2m_\rho^2}\right] \\
2\mathrm{Re}\overline{[\mathcal{M}_a^*\mathcal{M}_c]} &= \frac{8e^2g_{\rho\pi\pi}^2}{(t-m_\pi^2)}\left[(s-2m_\pi^2)-\frac{(m_\pi^2+m_\rho^2-u)(m_\pi^2+m_\rho^2-t)}{2m_\rho^2}\right] \\
2\mathrm{Re}\overline{[\mathcal{M}_b^*\mathcal{M}_c]} &= \frac{8e^2g_{\rho\pi\pi}^2}{(u-m_\pi^2)}\left[(s-2m_\pi^2)-\frac{(m_\pi^2+m_\rho^2-u)(m_\pi^2+m_\rho^2-t)}{2m_\rho^2}\right]
\end{aligned}
$$

$$
\underline{(2)\ \pi^0(p_1)+\pi^\pm(p_2)\ \rightarrow\ \rho^\pm(p_3)+\gamma(p_4)}
$$

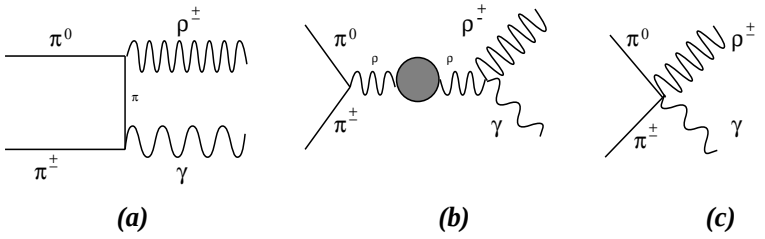

Figure 14: Feynman diagrams for $\pi^0\pi^\pm \rightarrow \rho^\pm\gamma$

$$
\begin{aligned}
\mathcal{M}_\dashv &= \frac{4eg_{\rho\pi\pi}}{(t-m_\pi^2)}p_{1\mu}p_{2\nu}\epsilon^{*\mu}(p_3)\epsilon^{*\nu}(p_4) \\
\mathcal{M}_\lfloor &= -\frac{eg_{\rho\pi\pi}}{(s-m_\rho^2+im_\rho\Gamma_\rho)}(p_1-p_2)^\mu \\
&\quad \times\left[2p_{4\nu}g_{\mu\lambda}-2p_{3\lambda}g_{\mu\nu}+(p_3-p_4)_\mu g_{\nu\lambda}\right]\epsilon^{*\nu}(p_3)\epsilon^{*\lambda}(p_4) \\
\mathcal{M}_\rfloor &= eg_{\rho\pi\pi}g_{\mu\nu}\epsilon^{*\mu}(p_3)\epsilon^{*\nu}(p_4)
\end{aligned}
$$

$$
\begin{aligned}
\overline{|\mathcal{M}_a|^2} &= \frac{16e^2g_{\rho\pi\pi}^2}{(t-m_\pi^2)^2}\,m_\pi^2\left[m_\pi^2-\frac{(m_\pi^2+m_\rho^2-t)^2}{4m_\rho^2}\right] \\
\overline{|\mathcal{M}_b|^2} &= \frac{e^2g_{\rho\pi\pi}^2}{\left[(s-m_\rho^2)^2+m_\rho^2\Gamma_\rho^2\right]}\left[2(t-u)^2+(4m_\pi^2-s)\left\{4m_\rho^2-\frac{(s-m_\rho^2)^2}{m_\rho^2}\right\}\right] \\
\overline{|\mathcal{M}_c|^2} &= 3e^2g_{\rho\pi\pi}^2
\end{aligned}
$$

$$
\begin{aligned}
2\mathrm{Re}\overline{[\mathcal{M}_a^*\mathcal{M}_b]} &= \frac{4e^2g_{\rho\pi\pi}^2(s-m_\rho^2)}{(t-m_\pi^2)[(s-m_\rho^2)^2+m_\rho^2\Gamma_\rho^2]}\left[2m_\pi^2(t-u)-s(s-4m_\pi^2)\right. \\
&\quad \left.+\frac{(s-4m_\pi^2)(s-m_\rho^2)(m_\pi^2+m_\rho^2-t)}{2m_\rho^2}\right]
\end{aligned}
$$

$$
\begin{aligned}
2\mathrm{Re}\overline{[\mathcal{M}_a^*\mathcal{M}_c]} &= \frac{4e^2g_{\rho\pi\pi}^2}{(t-m_\pi^2)}\left[(s-2m_\pi^2)-\frac{(m_\pi^2+m_\rho^2-u)(m_\pi^2+m_\rho^2-t)}{2m_\rho^2}\right] \\
2\mathrm{Re}\overline{[\mathcal{M}_b^*\mathcal{M}_c]} &= \frac{e^2g_{\rho\pi\pi}^2}{m_\rho^2}\frac{(t-u)(5m_\rho^2-s)(s-m_\rho^2)}{[(s-m_\rho^2)^2+m_\rho^2\Gamma_\rho^2]}
\end{aligned}
$$

$$\underline{(3)\ \pi^\pm(p_1)+\rho^0(p_2)\ \rightarrow\ \pi^\pm(p_3)+\gamma(p_4)}$$

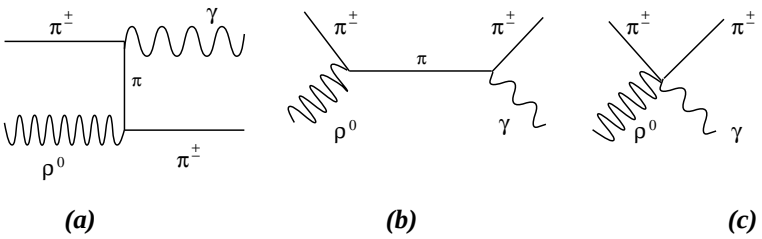

Figure 15: Feynman diagrams for $\pi^\pm\rho^0\ \rightarrow\ \pi^\pm\,\gamma$

$$
\begin{aligned}
\mathcal{M}_{\dashv} &= \frac{4eg_{\rho\pi\pi}}{(u-m_\pi^2)}p_{1\mu}p_{3\nu}\epsilon^\nu(p_2)\epsilon^{*\mu}(p_4) \\
\mathcal{M}_{\lfloor} &= \frac{4eg_{\rho\pi\pi}}{(s-m_\pi^2)}p_{1\mu}p_{3\nu}\epsilon^\mu(p_2)\epsilon^{*\nu}(p_4) \\
\mathcal{M}_{\rfloor} &= -2eg_{\rho\pi\pi}g_{\mu\nu}\epsilon^\mu(p_2)\epsilon^{*\nu}(p_4)
\end{aligned}
$$

$$
\begin{aligned}
\overline{|\mathcal{M}_a|^2} &= \frac{16e^2g_{\rho\pi\pi}^2}{3(u-m_\pi^2)^2}\,m_\pi^2\left[m_\pi^2-\frac{(m_\pi^2+m_\rho^2-u)^2}{4m_\rho^2}\right] \\
\overline{|\mathcal{M}_b|^2} &= \frac{16e^2g_{\rho\pi\pi}^2}{3(s-m_\pi^2)^2}\,m_\pi^2\left[m_\pi^2-\frac{(m_\pi^2+m_\rho^2-s)^2}{4m_\rho^2}\right] \\
\overline{|\mathcal{M}_c|^2} &= 4e^2g_{\rho\pi\pi}^2
\end{aligned}
$$

$$
\begin{aligned}
2\mathrm{Re}\overline{[\mathcal{M}_a^*\mathcal{M}_b]} &= \frac{4e^2g_{\rho\pi\pi}^2(t-2m_\pi^2)}{3(u-m_\pi^2)(s-m_\pi^2)}\left[(t-2m_\pi^2)-\frac{(m_\pi^2+m_\rho^2-s)(m_\pi^2+m_\rho^2-u)}{2m_\rho^2}\right] \\
2\mathrm{Re}\overline{[\mathcal{M}_a^*\mathcal{M}_c]} &= \frac{4e^2g_{\rho\pi\pi}^2}{3(u-m_\pi^2)}\left[(t-2m_\pi^2)-\frac{(m_\pi^2+m_\rho^2-u)(m_\pi^2+m_\rho^2-s)}{2m_\rho^2}\right] \\
2\mathrm{Re}\overline{[\mathcal{M}_b^*\mathcal{M}_c]} &= \frac{4e^2g_{\rho\pi\pi}^2}{3(s-m_\pi^2)}\left[(t-2m_\pi^2)-\frac{(m_\pi^2+m_\rho^2-s)(m_\pi^2+m_\rho^2-u)}{2m_\rho^2}\right]
\end{aligned}
$$

$$\underline{(4)\ \pi^\pm(p_1)+\rho^\mp(p_2)\ \rightarrow\ \pi^0(p_3)+\gamma(p_4)}$$

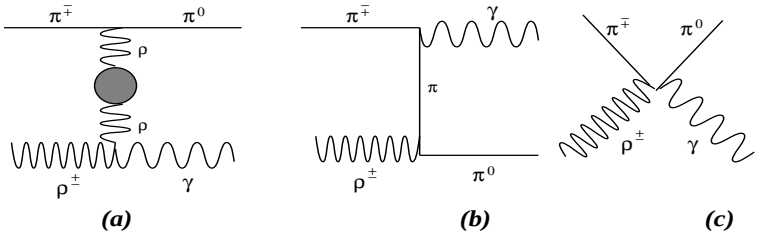

Figure 16: Feynman diagrams for $\pi^{\pm}\rho^{\mp} \rightarrow \pi^0\,\gamma$

$$
\begin{aligned}
\mathcal{M}_{\dashv} &= \frac{e g_{\rho\pi\pi}}{(t - m_\rho^2 + i m_\rho \Gamma_\rho)} (p_1 + p_3)^\mu \\
&\quad \times \left[2p_{4\nu} g_{\mu\lambda} + 2p_{2\lambda} g_{\mu\nu} - (p_2 + p_4)_\mu g_{\nu\lambda} \right] \epsilon^\nu(p_2) \epsilon^{*\lambda}(p_4) \\
\mathcal{M}_{\lfloor} &= -\frac{4 e g_{\rho\pi\pi}}{(u - m_\pi^2)} p_{1\mu} p_{3\nu} \epsilon^\nu(p_2) \epsilon^{*\mu}(p_4) \\
\mathcal{M}_{\rfloor} &= e g_{\rho\pi\pi} g_{\mu\nu} \epsilon^\mu(p_2) \epsilon^{*\nu}(p_4)
\end{aligned}
$$

$$
\begin{aligned}
\overline{|\mathcal{M}_a|^2} &= \frac{e^2 g_{\rho\pi\pi}^2}{3\left[(t - m_\rho^2)^2 + m_\rho^2 \Gamma_\rho^2\right]} \left[2(s-u)^2 + (4m_\pi^2 - t) \left\{ 4m_\rho^2 - \frac{(t - m_\rho^2)^2}{m_\rho^2} \right\} \right] \\
\overline{|\mathcal{M}_b|^2} &= \frac{16 e^2 g_{\rho\pi\pi}^2}{3(u - m_\pi^2)^2} m_\pi^2 \left[m_\pi^2 - \frac{(m_\pi^2 + m_\rho^2 - u)^2}{4m_\rho^2} \right] \\
\overline{|\mathcal{M}_c|^2} &= e^2 g_{\rho\pi\pi}^2
\end{aligned}
$$

$$
\begin{aligned}
2\mathrm{Re}\overline{[\mathcal{M}_a^* \mathcal{M}_b]} &= \frac{4 e^2 g_{\rho\pi\pi}^2 (t - m_\rho^2)}{3(u - m_\pi^2)[(t - m_\rho^2)^2 + m_\rho^2 \Gamma_\rho^2]} \left[2m_\pi^2 (u - s) - t(t - 4m_\pi^2) \right. \\
&\quad \left. + \frac{(t - 4m_\pi^2)(t - m_\rho^2)(m_\pi^2 + m_\rho^2 - u)}{2m_\rho^2} \right] \\
2\mathrm{Re}\overline{[\mathcal{M}_a^* \mathcal{M}_c]} &= \frac{e^2 g_{\rho\pi\pi}^2}{3m_\rho^2} \frac{(u - s)(5m_\rho^2 - t)(t - m_\rho^2)}{[(t - m_\rho^2)^2 + m_\rho^2 \Gamma_\rho^2]} \\
2\mathrm{Re}\overline{[\mathcal{M}_b^* \mathcal{M}_c]} &= \frac{4 e^2 g_{\rho\pi\pi}^2}{3(u - m_\pi^2)} \left[(t - 2m_\pi^2) - \frac{(m_\pi^2 + m_\rho^2 - s)(m_\pi^2 + m_\rho^2 - u)}{2m_\rho^2} \right]
\end{aligned}
$$

$$\underline{(5)\ \pi^0(p_1) + \rho^{\pm}(p_2) \rightarrow \pi^{\pm}(p_3) + \gamma(p_4)}$$

$$
\mathcal{M}_{\dashv} = -\frac{e g_{\rho\pi\pi}}{(t - m_\rho^2 + i m_\rho \Gamma_\rho)} (p_1 + p_3)^\mu
$$

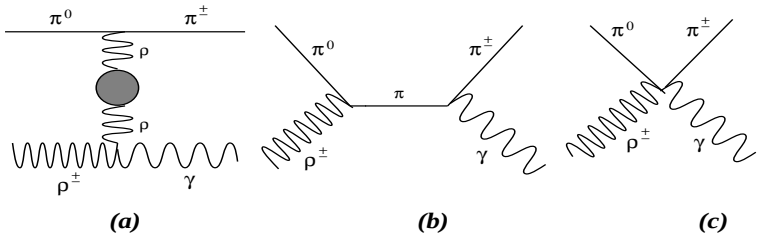

Figure 17: Feynman diagrams for $\pi^0\rho^\pm \to \pi^\pm\gamma$

$$\times\left[2p_{4\nu}g_{\mu\lambda}+2p_{2\lambda}g_{\mu\nu}-(p_2+p_4)_\mu g_{\nu\lambda}\right]\epsilon^\nu(p_2)\epsilon^{*\lambda}(p_4)$$

$$\begin{aligned}
\mathcal{M}_{\lfloor} &= -\frac{4eg_{\rho\pi\pi}}{(s-m_\pi^2)}p_{1\mu}p_{3\nu}\epsilon^\mu(p_2)\epsilon^{*\nu}(p_4)\\
\mathcal{M}_{\rfloor} &= eg_{\rho\pi\pi}g_{\mu\nu}\epsilon^\mu(p_2)\epsilon^{*\nu}(p_4)
\end{aligned}$$

$$\begin{aligned}
\overline{|\mathcal{M}_a|^2} &= \frac{e^2g_{\rho\pi\pi}^2}{3\left[(t-m_\rho^2)^2+m_\rho^2\Gamma_\rho^2\right]}\left[2(s-u)^2+(4m_\pi^2-t)\left\{4m_\rho^2-\frac{(t-m_\rho^2)^2}{m_\rho^2}\right\}\right]\\
\overline{|\mathcal{M}_b|^2} &= \frac{16e^2g_{\rho\pi\pi}^2}{3(s-m_\pi^2)^2}\,m_\pi^2\left[m_\pi^2-\frac{(m_\pi^2+m_\rho^2-s)^2}{4m_\rho^2}\right]\\
\overline{|\mathcal{M}_c|^2} &= e^2g_{\rho\pi\pi}^2
\end{aligned}$$

$$\begin{aligned}
2\mathrm{Re}\overline{[\mathcal{M}_a^*\mathcal{M}_b]} &= \frac{4e^2g_{\rho\pi\pi}^2(t-m_\rho^2)}{3(s-m_\pi^2)[(t-m_\rho^2)^2+m_\rho^2\Gamma_\rho^2]}\left[2m_\pi^2(s-u)-t(t-4m_\pi^2)\right.\\
&\qquad\left.+\frac{(t-4m_\pi^2)(t-m_\rho^2)(m_\pi^2+m_\rho^2-s)}{2m_\rho^2}\right]\\
2\mathrm{Re}\overline{[\mathcal{M}_a^*\mathcal{M}_c]} &= \frac{e^2g_{\rho\pi\pi}^2}{3m_\rho^2}\frac{(s-u)(5m_\rho^2-t)(t-m_\rho^2)}{[(t-m_\rho^2)^2+m_\rho^2\Gamma_\rho^2]}\\
2\mathrm{Re}\overline{[\mathcal{M}_b^*\mathcal{M}_c]} &= \frac{4e^2g_{\rho\pi\pi}^2}{3(s-m_\pi^2)}\left[(t-2m_\pi^2)-\frac{(m_\pi^2+m_\rho^2-u)(m_\pi^2+m_\rho^2-s)}{2m_\rho^2}\right]
\end{aligned}$$

$\underline{(6)\ \rho(p_1)\ \to\ \pi(p_2)\,\pi(p_3)\gamma(p_4),\ \omega(p_1)\ \to\ \pi(p_2)\,\gamma(p_3)}$

$$\begin{aligned}
\mathcal{M}_{\dashv} &= -\frac{4eg_{\rho\pi\pi}}{(t-m_\pi^2)}p_{3\mu}p_{2\nu}\epsilon^\mu(p_1)\epsilon^{*\nu}(p_4)\\
\mathcal{M}_{\lfloor} &= -\frac{4eg_{\rho\pi\pi}}{(s-m_\pi^2)}p_{2\mu}p_{3\nu}\epsilon^\mu(p_1)\epsilon^{*\nu}(p_4)\\
\mathcal{M}_{\rfloor} &= -2eg_{\rho\pi\pi}g_{\mu\nu}\epsilon^\mu(p_1)\epsilon^{*\nu}(p_4)
\end{aligned}$$

$$\overline{|\mathcal{M}_a|^2} = \frac{16e^2g_{\rho\pi\pi}^2}{3(t-m_\pi^2)^2}\,m_\pi^2\left[m_\pi^2-\frac{(m_\pi^2+m_\rho^2-t)^2}{4m_\rho^2}\right]$$

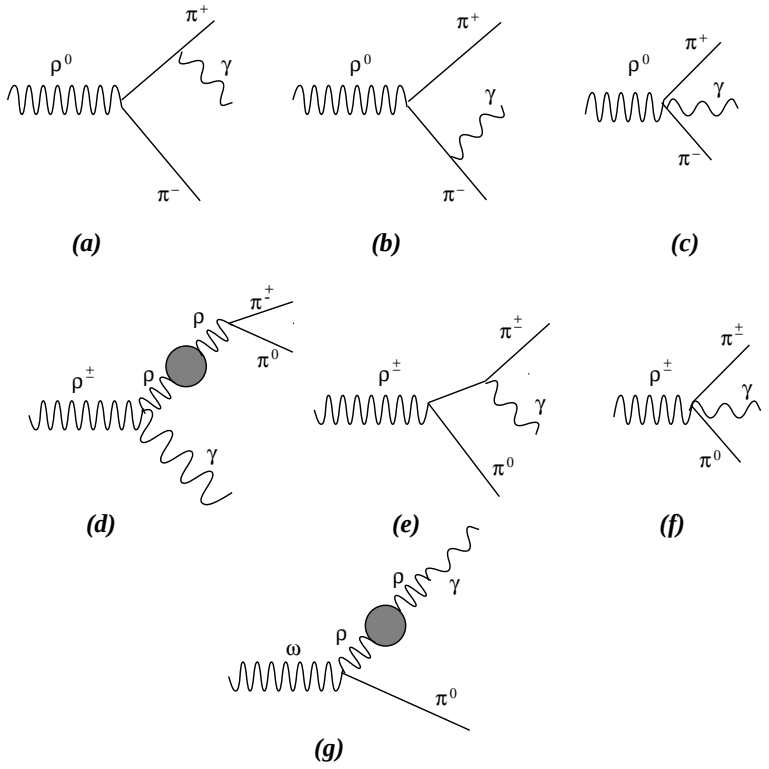

Figure 18: Feynman diagrams for vector meson decays.

$$\begin{aligned}
\overline{|\mathcal{M}_b|^2} &= \frac{16e^2g_{\rho\pi\pi}^2}{3(s-m_\pi^2)^2}\,m_\pi^2\left[m_\pi^2-\frac{(m_\pi^2+m_\rho^2-s)^2}{4m_\rho^2}\right]\\
\overline{|\mathcal{M}_c|^2} &= 4e^2g_{\rho\pi\pi}^2
\end{aligned}$$

$$\begin{aligned}
2\mathrm{Re}\overline{[\mathcal{M}_a^*\mathcal{M}_b]} &= \frac{8e^2g_{\rho\pi\pi}^2(u-2m_\pi^2)}{3(t-m_\pi^2)(s-m_\pi^2)}\left[(u-2m_\pi^2)-\frac{(m_\pi^2+m_\rho^2-t)(m_\pi^2+m_\rho^2-s)}{2m_\rho^2}\right]\\
2\mathrm{Re}\overline{[\mathcal{M}_a^*\mathcal{M}_c]} &= \frac{8e^2g_{\rho\pi\pi}^2}{3(t-m_\pi^2)}\left[(u-2m_\pi^2)-\frac{(m_\pi^2+m_\rho^2-s)(m_\pi^2+m_\rho^2-t)}{2m_\rho^2}\right]\\
2\mathrm{Re}\overline{[\mathcal{M}_b^*\mathcal{M}_c]} &= \frac{8e^2g_{\rho\pi\pi}^2}{3(s-m_\pi^2)}\left[(u-2m_\pi^2)-\frac{(m_\pi^2+m_\rho^2-s)(m_\pi^2+m_\rho^2-t)}{2m_\rho^2}\right]
\end{aligned}$$

$$\begin{aligned}
\mathcal{M}_{\lceil} &= -\frac{eg_{\rho\pi\pi}}{(u-m_\rho^2+im_\rho\Gamma_\rho)}(p_2-p_3)^\mu\\
&\quad\times\left[2p_{4\nu}g_{\mu\lambda}+2p_{1\lambda}g_{\mu\nu}-(p_1+p_4)_\mu g_{\nu\lambda}\right]\epsilon^\nu(p_1)\epsilon^{*\lambda}(p_4)\\
\mathcal{M}_{\rceil} &= \frac{4eg_{\rho\pi\pi}}{(t-m_\pi^2)}p_{3\mu}p_{2\nu}\epsilon^\mu(p_1)\epsilon^{*\nu}(p_4)\\
\mathcal{M}_{\{} &= eg_{\rho\pi\pi}g_{\mu\nu}\epsilon^\mu(p_1)\epsilon^{*\nu}(p_4)
\end{aligned}$$

$$
\begin{aligned}
\overline{|\mathcal{M}_d|^2} &= \frac{e^2 g_{\rho\pi\pi}^2}{3\left[(u-m_\rho^2)^2+m_\rho^2\Gamma_\rho^2\right]}\left[2(t-s)^2+(4m_\pi^2-u)\left\{4m_\rho^2-\frac{(u-m_\rho^2)^2}{m_\rho^2}\right\}\right] \\
\overline{|\mathcal{M}_e|^2} &= \frac{16e^2 g_{\rho\pi\pi}^2}{3(t-m_\pi^2)^2}\,m_\pi^2\left[m_\pi^2-\frac{(m_\pi^2+m_\rho^2-t)^2}{4m_\rho^2}\right] \\
\overline{|\mathcal{M}_f|^2} &= e^2 g_{\rho\pi\pi}^2
\end{aligned}
$$

$$
\begin{aligned}
2\mathrm{Re}\overline{[\mathcal{M}_d^*\mathcal{M}_e]} &= \frac{4e^2 g_{\rho\pi\pi}^2(u-m_\rho^2)}{3(t-m_\pi^2)[(u-m_\rho^2)^2+m_\rho^2\Gamma_\rho^2]}\left[2m_\pi^2(t-s)-u(u-4m_\pi^2)\right. \\
&\quad \left.+\frac{(u-4m_\pi^2)(u-m_\rho^2)(m_\pi^2+m_\rho^2-t)}{2m_\rho^2}\right] \\
2\mathrm{Re}\overline{[\mathcal{M}_d^*\mathcal{M}_f]} &= \frac{e^2 g_{\rho\pi\pi}^2}{3m_\rho^2}\frac{(t-s)(5m_\rho^2-u)(u-m_\rho^2)}{[(u-m_\rho^2)^2+m_\rho^2\Gamma_\rho^2]} \\
2\mathrm{Re}\overline{[\mathcal{M}_e^*\mathcal{M}_f]} &= \frac{4e^2 g_{\rho\pi\pi}^2}{3(t-m_\pi^2)}\left[(u-2m_\pi^2)-\frac{(m_\pi^2+m_\rho^2-t)(m_\pi^2+m_\rho^2-s)}{2m_\rho^2}\right]
\end{aligned}
$$

$$
\mathcal{M}_\} = \left(\frac{\rceil\}_{\omega\pi\rho}\Updownarrow_\rho^\in}{\Updownarrow_\pi\}_{\rho\pi\pi}}\right)\epsilon_{\mu\nu\alpha\beta}\sqrt{}^{\mu}_{\infty}\sqrt{}^{\alpha}_{\ni}\left(\frac{-\}^{\sigma\beta}+\sqrt{}^{\sigma}_{\ni}\sqrt{}^{\beta}_{\ni}/\Updownarrow_\rho^\in}{\sqrt{}^{\in}_{\ni}-\Updownarrow_\rho^\in+\rangle\Updownarrow_\rho-_\rho}\right)\epsilon^\nu(\sqrt{}^{}_{\infty})\epsilon_\sigma^*(\sqrt{}^{}_{\ni})
$$

$$
|\mathcal{M}_\}|^\in = \frac{\in\pi\alpha}{\ni}\left(\frac{\}_{\omega\pi\rho}}{\}_{\rho\pi\pi}}\right)^\in\frac{\Updownarrow_\rho^\triangle}{\Updownarrow_\pi^\in}\frac{(\Updownarrow_\omega^\in-\Updownarrow_\pi^\in)^\in}{[(\sqcup-\Updownarrow_\rho^\in)^\in+\Updownarrow_\rho^\in-_\rho^\in]}
$$

Appendix - III

In this appendix we define various parameters and integration limits which appeared in Eq. (30).

$$
\begin{aligned}
a &= -(s+t-m_2^2-m_3^2)^2 \\
b &= E_1(s+t-m_2^2-m_3^2)(m_2^2-t)+E[(s+t-m_2^2-m_3^2)(s-m_1^2-m_2^2) \\
&\quad -2m_1^2(m_2^2-t)] \\
c &= -E_1^2(m_2^2-t)^2-2E_1E[2m_2^2(s+t-m_2^2-m_3^2)-(m_2^2-t)(s-m_1^2-m_2^2)] \\
&\quad -E^2[(s-m_1^2-m_2^2)^2-4m_1^2m_2^2]-(s+t-m_2^2-m_3^2)(m_2^2-t) \\
&\quad \times(s-m_1^2-m_2^2)+m_2^2(s+t-m_2^2-m_3^2)^2+m_1^2(m_2^2-t)^2 \\
E_{1\min} &= \frac{(s+t-m_2^2-m_3^2)}{4E}+\frac{Em_1^2}{s+t-m_2^2-m_3^2}
\end{aligned}
$$

$$E_{2\min} = \frac{Em_2^2}{m_2^2 - t} + \frac{m_2^2 - t}{4E}$$
$$E_{2\max} = -\frac{b}{a} + \frac{\sqrt{b^2 - ac}}{a}$$

References

[1] B. Müller, The Physics of Quark-Gluon Plasma, Springer, Heidelberg 1985.

[2] R. C. Hwa (ed.), Quark-Gluon Plasma, World Scientific, Singapore 1990.

[3] C. Y. Wong, Introduction to High Energy Heavy-Ion Collisions, World Scientific Singapore 1994.

[4] J. Alam, S. Raha, and B. Sinha, Phys. Rep. **273** 243 (1996).

[5] S. Bonometto and O. Pantano, Phys. Rep. **228** 175 (1993).

[6] R. D. Pisarski in Workshop on Finite Temperature QCD and Quark-Gluon Transport Theory, Wuhan, PRC April 1994.

[7] B. D. Serot and J. D. Walecka, Advances in Nuclear Physics Vol. 16 Plenum Press, New York 1986.

[8] H. C. Jean, J. Piekarewicz and A. G. Williams, Phys. Rev. **C49**, 1981(1994).

[9] T. Hadsuda, Y. Koike and S. H. Lee, Phys. Rev. **D47**, 1225(1993).

[10] H. Shiomi and T. Hatsuda, Phys. Lett. **B334** 281(1994).

[11] A. Das, Finite Temperature Field Theory, World Scientific, Singapore 1997.

[12] M. B. Kislinger and P. D. Morley, Phy. Rev. **D13** 2771 (1976).

[13] J. I. Kapusta, Finite Temperature Field Theory, Cambridge University Press, Cambridge 1989.

[14] C. Song, P. W. Xia, and C. M. Ko, Phys. Rev. **C52** 408 (1995).

[15] C. Gale and J. I. Kapusta, Nucl. Phys. **B357** 65 (1991).

[16] H. A. Weldon, Phys. Rev. **D28** 2007 (1983).

[17] A. K. Dutt-Majumdar, J. Alam, B. Dutta-Roy, and B. Sinha, Phys. Lett. **B378** 35 (1996).

[18] R. Rapp and J. Wambach, Phys. Rev. **C53** 3057 (1996).

[19] Z. Aouissat, G. Chanfray, P. Schuck, and G. Welke, Z. Phys. **A340** 347 (1991).

[20] H. W. Barz, G. F. Bertsch, P. Danielewicz, and H, Schulz, Phys. Lett **B275** 19 (1992).

[21] P. Lichard, Private Communication.

[22] J. I. Kapusta, P. Lichard, and D. Seibert, Phys. Rev. **D44** 2774 (1991).

[23] J. J. Sakurai, Currents and Mesons, The University of Chicago Press, Chicago, 1969.

[24] C. Gale and J. I. Kapusta, Phys. Rev. **C35** 2107 (1987).

[25] R. Machleidt, K. Holinde, and Ch. ELster, Phys. Rep. **149** 1 (1987).

[26] R. J. Furnstahl and T. Hatsuda, Phys. Rev. **D42** 1744 (1990).

[27] C. Adami, T. Hatsuda, and I. Zahed, Phys. Rev. **D43** 921 (1991).

[28] T. Hatsuda, Nucl. Phys. **A544** 27c (1992).

[29] G. E. Brown, Nucl. Phys. **A522** 397c (1991).

[30] G. E. Brown and M. Rho, Phys. Rev. Lett. **66** 2720 (1991).

[31] A. Bhattacharyya, J. Alam, S. Raha and B. Sinha, Int. J. Mod. Phys. **A** (in press).

[32] J. D. Bjorken, Phys. Rev. **D27** 140 (1983).

[33] S. Sarkar *et al* to be published.